SEVENTEENTH EUROPEAN ROTORCRAFT FORUM

Paper No. 91 - 61

BVI IMPULSIVE NOISE REDUCTION BY HIGHER HARMONIC PITCH CONTROL: RESULTS OF A SCALED MODEL ROTOR EXPERIMENT IN THE DNW

W.R. SPLETTSTOESSER, K.-J. SCHULTZ, R. KUBE
DLR, BRAUNSCHWEIG, GERMANY

T.F. BROOKS, E.R. BOOTH, JR.
NASA LaRC, HAMPTON, VA, USA

G. NIESL
MBB, OTTOBRUNN, GERMANY

O. STREBY
AEROSPATIALE, MARIGNANE, FRANCE

SEPTEMBER 24 - 26, 1991

Berlin, Germany

BVI IMPULSIVE NOISE REDUCTION BY HIGHER HARMONIC PITCH CONTROL:
RESULTS OF A SCALED MODEL ROTOR EXPERIMENT IN THE DNW

Wolf R. Splettstoesser, Klaus-J. Schultz, Roland Kube
DLR Research Center Braunschweig, Germany

Thomas F. Brooks and Earl R. Booth, Jr.
NASA Langley Research Center, Hampton VA, USA

Georg Niesl
MBB Ottobrunn, Germany

Olivier Streby
Aerospatiale Marignane, France

ABSTRACT

A model rotor acoustics test was performed to examine the benefit of higher harmonic control (HHC) of blade pitch to reduce blade-vortex interaction (BVI) impulsive noise. A dynamically scaled, four-bladed, rigid rotor model, a 40% replica of the BO-105 main rotor, was tested in the German Dutch Wind Tunnel (Deutsch-Niederländischer Windkanal, DNW). Acoustic measurements were made in a large plane underneath the rotor employing a traversing in-flow microphone array in the anechoic environment of the open test section. Noise characteristics and noise directivity patterns as well as vibratory loads were measured and used to demonstrate the changes when different HHC schedules (different modes, amplitudes, phases) were applied. Dramatic changes of the acoustic signatures and the noise radiation directivity with HHC phase variations are found. Compared to the baseline conditions (without HHC), significant mid-frequency noise reductions of locally 6 dB are obtained for low speed descent conditions where BVI is most intense. For other rotor operating conditions with less intense BVI there is less or no benefit from the use of HHC. Low frequency loading noise and vibratory loads, especially at optimum noise reduction control settings, are found to increase.

SYMBOLS

a_o speed of sound, m/s

C_T Rotor thrust coefficient, thrust/ $\rho \pi R^2 (\Omega R)^2$

f frequency, 1/sec

f_{bp} blade passage frequency, number of blades multiplied by $\Omega/2\pi$

GF   vibration quality criterion, rms value of 4/rev components of balance forces and moments, normalized to baseline GF without HHC, %

M_H hover tip Mach number, $\Omega R/a_o$

nP   n'th harmonic of rotor rotational period

R   rotor radius, m

r   radial distance from hub, m

SP   sound pressure, Pa

SPL   sound pressure level, pressure reference is 20 µPa, dB

X   streamwise coordinate relative to hub, positive downstream, m

X_w streamwise location of traversing array relative to hub, m

Y   cross stream coordinate relative to hub, positive on advancing side, m

Z   vertical cross stream coordinate relative to hub, positive above hub, m

α rotor tip path plane angle referenced to tunnel streamwise axis, deg

α' effective α corrected for free jet wind tunnel effects, deg

$\ominus$ calculated full-scale helicopter flight path angle, positive in descent, deg

θ_c amplitude of higher harmonic pitch at ψ_c, deg

Φ phase angle of higher harmonic pitch, referenced to positive θ_c for reference blade passing zero azimuth ($\psi = 0°$), deg

μ advance ratio, tunnel flow velocity/ΩR

ρ air density, kg/m³

ψ blade azimuth angle, deg

ψ_c blade azimuth angle selected for θ_c, deg

Ω rotor rotational speed, rad/sec

INTRODUCTION

Blade-vortex interaction (BVI) impulsive noise of helicopters is considered a matter of major concern for the acceptability of rotorcraft in densely populated areas and has become an important subject of rotor acoustics research in recent years. The pulse-type noise due to BVI originates from the unsteady aerodynamic interaction between a lift generating blade and the vortex system shed by preceding blades. This phenomenon is generally observed during low speed descent, especially landing approach, and during manoeuvre flight condition, when the

displacements between the rolled-up tip vor-
tices and the rotor plane become extremely
small. When BVI occurs, this noise mechanism
dominates the noise radiation in the mid-
frequency range to which human subjective
response is most sensitive.

Earlier experimental work on BVI noise was
performed on full-scale and model-scale
helicopter rotors in order to determine the
rotor operating regimes for BVI (Refs 1-3),
the primary parameters affecting BVI noise
generation and radiation, as well as the
model-to-full-scale acoustic scaling condi-
tions (Refs 4-6). Advancing and retreating
side BVI source locations were identified in
the first and fourth quadrant of the rotor
plane (Refs 7,8) and were found to be most
intense where the blade and the vortex axes
are close to parallel (between 45° and 75°
and about 300° azimuth angle, respectively).

A BVI noise reduction hypothesis (Ref 9)
suggested that decreases in blade lift, vor-
tex strength, and/or increases in blade vor-
tex separation distance at the blade-vortex
encounters should help to reduce the effect
of BVI on the unsteady blade loads and thus
on noise. The technique of higher harmonic
control (HHC) of the blade pitch, histori-
cally developed for vibration control (Refs
10-13), was thought to be useful for manipu-
lating those parameters. The HHC noise re-
duction concept is sketched in Fig 1, which
illustrates rotor blades undergoing higher
harmonic pitch variations. The amplitude and
proper phasing of such pitch controls at the
azimuthal locations of the most intense BVI
encounters and at upstream locations, where
the encountering vortex is being generated,
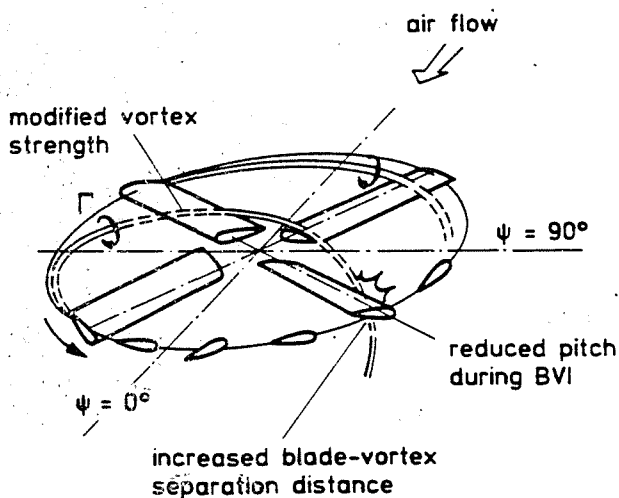would be considered to be important to the
noise problem.

air flow

modified vortex
strength

ψ = 90°

reduced pitch
during BVI

ψ = 0°

increased blade-vortex
separation distance

Fig 1 Illustration of noise reduction concept.

Initial findings from two independent re-
search programs (Refs 14,15,16) indicated a
considerable noise reduction benefit of HHC.
Based on a pilot experiment in the DNW
closed test section, a pre-test of the pre-
sent study, Ref 14 reported that significant
BVI noise reductions (4-5 dB) for a limited
number of typical low speed descent condi-
tions were found, however at the cost of in-
creased vibration levels. Three HHC pitch
schedules (3P, 4P, 5P) were examined and
were found to produce similar noise reduc-
tions and somewhat similar vibration re-

sults. Rotor performance and wake calcula-
tions including higher harmonic pitch ef-
fects were reported for one flight condi-
tion, which indicated that local blade load-
ing decreased and blade-vortex displacement
increased at BVI source locations for
maximum BVI noise reduction, which would be
consistent with the noise reduction hypothe-
sis described above. However, vortex
strength was calculated to be increased. The
results of a major HHC acoustic test in the
Langley Transonic Dynamics Tunnel (TDT), re-
ported in Refs 15 and 16, were quite consis-
tent with the Ref 14 results. The particular
prescribed pitch schedule used for HHC was a
4P collective pitch control superimposed on
the normal cyclic trim pitch. Uniquely, the
acoustic testing was conducted in a heavy
gas (Freon-12) flow medium, instead of air,
and the reverberant field of the hard wall
tunnel test section was used to advantage by
choosing a sound power measurement approach.
Significant BVI (mid-frequency) noise reduc-
tions (5-6 dB) were found for low-speed de-
scent conditions where BVI is most intense.
For other flight conditions noise was found
to increase with use of HHC. On the negative
side, the mid- frequency noise reductions
due to HHC were reported to be accompanied
by increased low frequency noise and vibra-
tion levels. Similar BVI noise reductions
and trends were observed during an active
vibration control flight test program on an
experimental SA349 Gazelle helicopter (Ref
17).

The present paper reports on results of a
three-nation cooperative model rotor test in
the DNW making use of the experience gained
by research personnel of the United States,
France and Germany during the HHC acoustic
tests referenced above. This rotor test was
designed to further establish the noise re-
duction potential of HHC by the determina-
tion of the noise directivity. The ex-
perimental approach involved the measurement
of noise and vibration with and without pre-
scribed HHC blade pitch inputs, which com-
prised 3P, 4P, 5P pitch schedules and some
combined (mixed) modes. For the first time
an HHC rotor acoustic test was performed in
an anechoic environment, which allowed meas-
urements of uncontaminated BVI noise signa-
tures on a large plane underneath the rotor.
By comparing the related sound fields the
changes of the acoustic waveform shapes and
the radiation directivity pattern due to
HHC, as well as the noise reduction benefit,
are demonstrated.

EXPERIMENT

Wind Tunnel and Rotor Test Stand

The test program was conducted in the open
test section of the German Dutch Wind Tunnel
(Deutsch-Niederländischer-Windkanal, DNW)
located in The Netherlands. The open confi-
guration employs an 8m x 6m nozzle that pro-
vides a free jet to the test section of 19m
length. The open test section is surrounded
by a large anechoic chamber with a nominal
cut-off frequency of 80 Hz (Ref 18). The DLR
model rotor test stand together with the
traversing in-flow microphone array is shown
installed in the DNW open test section in
Fig 2. The rotor test stand was housed in an
acoustically insulated fiberglas fuselage
and was attached to the computer controlled,

hydraulic sting support mechanism. Fuselage
and sting were covered with a sound absorp-
tive lining to minimize acoustic reflec-
tions. The rotor was driven by a hydraulic
motor (100 kW) and controlled by three
equally spaced electro-hydraulic actuators
providing both conventional (1 per revolu-
tion) and higher harmonic (3P, 4P, 5P) blade
pitch control. Details of rotor performance
and data acquisition/reduction are given in
Refs 19 and 20, and are summarized in Ref
21. The data acquisition system acquired
about 48 samples per rotor revolution from
each of the 64 sensors that allowed data
analysis in the frequency domain up to the
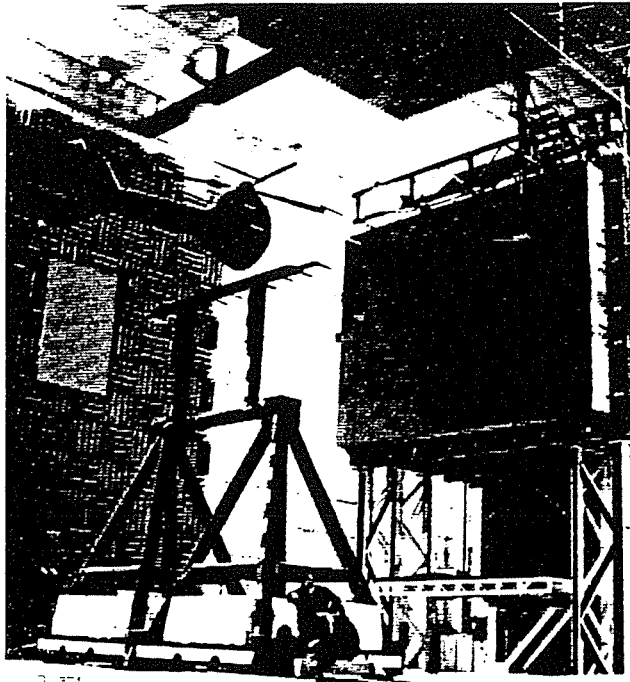9th rotor harmonic.

Fig 2 Rotor model and in-flow microphone array in-
stalled in the DNW open test section.

The rotor is a 40-percent, dynamically
scaled replica of a four-bladed, hingeless
BO-105 main rotor. The rotor diameter is 4m,
the blade cross section is a NACA 23012 air-
foil with the trailing edge modified to form
a 5mm-long tab to match the geometry of the
full-scale rotor. The rotor blades have a
chord length of 121mm, a linear twist of
-8°, and a standard rectangular tip. The
nominal rotor operating speed was 1050 rpm
giving a blade passage frequency (fbp) of 70
Hz and a hover tip Mach number of 0.64. No-
minal thrust coefficient was 0.0044. Further
details are given in Ref 19. Wind tunnel
corrections to the measured geometric shaft
angle (α) for the effect of the finite open
jet potential core were calculated with the
theory of Refs 22,23. The corrected flow an-
gle corresponding to the full-scale flight
condition is referred to as the tip-path-
plane angle, α'.

Acoustic Instrumentation and Data Acquisition

The acoustic instrumentation comprised an
eleven-microphone in-flow array mounted on a
traversing system (Fig 2) and three in-flow

microphones, two of which were mounted on
the starboard side (advancing side) of the
fuselage and one on the port side (retreat-
ing side). The microphones were 1/2-inch
pressure-type condensor microphones equipped
with standard nose cones. Microphone cali-
brations were performed with a sound level
calibrator on a daily base. In addition,
pure tone and white noise signals were re-
corded on each magnetic tape simultaneously
on all channels by signal insertion at the
tape recorder inputs. The microphone signals
were high-pass filtered at 4 Hz to remove
very low frequency content associated with
the free jet flow in the open test section.

The microphone array traverse system con-
sisted of a horizontal wing with its span
normal to the flow direction, with a useful
range in flow direction of 4m upstream and
4m downstream of the rotor hub. The micro-
phones were arranged symmetrically with re-
spect to the tunnel centerline, spaced 0.54m
apart, and nominally 2.4m below the rotor
hub. The microphone holders employed a vi-
bration isolating mounting. Wing and support
struts were covered with an open-cell foam
cut in an airfoil section shape. The sup-
porting structure was covered with a 0.1m-
thick foam lining, and the base was protect-
ed with 0.8m foam wedges. In Ref 21 details
on control, positioning, and alignment of
the array are given.

For measuring the radiated sound field on a
large plane (5.4m x 8m) underneath the ro-
tor, an advanced measurement technique was
applied, that allowed to reduce the data ac-
quisition time by a factor of about five at
twice the spatial resolution in flow direc-
tion compared to earlier measurements using
fixed streamwise traverse positions (Ref
21). The new "on-the-fly" data acquisition
technique employed a continuously, however
slowly moving microphone traverse with the
data acquisition started at preselected
streamwise locations. As shown in Fig 3 with
a spacing of 0.5m in flow direction, the
spatial resolution of the sound field was
187 measurement points (or about 0.25 m^2).
The traversing speed was chosen to be very
low (about 0.038 m/s) to approximate sta-
tionary measurements of the sound field. At
each of the 17 streamwise traverse positions
the data acquisition was initiated and
acoustic data for time periods of 30 rotor
revolutions (approx. 1.7s) were acquired
simultaneously with rotor and wind tunnel
operational data. During this data acquisi-
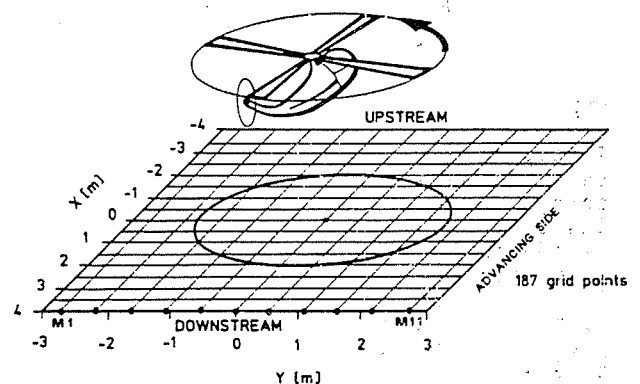tion period the traverse displacement was

Fig 3 Illustration of the acoustic measurement
plane, 1.2 R underneath the rotor hub.

very small with a marginal change in radiation angle of approximately one degree in major BVI noise radiation directions. Comparisons of instantaneous and averaged time signatures from "on-the-fly" and completely stationary measurements at fixed traverse positions did not show noticeable differences. Therefore, the new data acquisition technique is considered to provide high quality quasi-steady acoustic results in a very efficient way. A typical acoustic data acquisition cycle to measure the complete sound field (Fig 3) comprises microphone gain adjustments during the downstream travel of the microphone traverse, initiation of the analog recording system, and the measurement phase during the upstream movement of the microphone array with repeated digital data acquisition at (17) predetermined streamwise locations, giving a total cycle time of about 5 to 6 minutes.

Investigations into the data quality were performed in a pre-test phase by conducting tunnel background noise and reflection tests with all testing and model hardware (except the blades) installed in the test section. Background noise levels were found to be typically 20 dB lower in the frequency range dominated by rotor BVI noise. The blast test indicated no extraordinary reflections; if any they were typically 15 to 20 dB below the direct signals. The results were quite useful to identify regions where some microphones may be "shielded" by the fuselage. Additional topics regarding the high standard of data quality, like tunnel flow quality, rotor performance data, and the steadiness and repeatability of the rotor acoustic data are summarized for a very similar test set-up in Ref 21.

Data Reduction and Analysis

The microphone signals, the blade position reference signal (once-per-revolution signal) and the traverse position signal were synchronously digitized with 16-bit resolution to provide nominal 1024 samples per rotor revolution. This digitizing process was keyed to the 1024-per-revolution signal of the blade azimuth angle encoder, and provided a sample rate of about 18000 samples-per-second with antialiasing filters set at 9 kHz, that gave a useful frequency range between 4 Hz and 9000 Hz. Thirty rotor revolutions of real-time acoustic data were stored on computer disk with subsequent calculation of the averaged power spectrum using Fast Fourier Transform (FFT) software. Several noise metrics were calculated from these on-line results like A-weighted levels, perceived noise levels, and some linear band-pass levels. A very useful estimate of the BVI impulsive noise content was a mid-frequency noise level, comprising the acoustic energy from the 6th to the 40th harmonic of the blade passage frequency, f_{bp}. In a similar way a low frequency noise level representing the 1st to the 5th f_{bp} harmonic was calculated. For different metrics, contours of equal noise levels were generated on-line and plotted for the measurement plane. These contour plots immediately indicated the BVI noise directivity pattern and the change in directivity and intensity of the noise radiation when HHC was applied. Finally, a reduction of the vast amount of noise data to single noise descriptors was obtained by calculation of

an average (mid-frequency) BVI noise level and by determination of maximum mid-frequency noise levels for both advancing side BVI and retreating side BVI. This was accomplished by a search algorithm scanning through the sound field underneath the first, second and third quadrant of the rotor plane for the maximum of advancing side noise radiation and underneath the fourth quadrant for maximum retreating side BVI noise. These single value noise descriptors were found to be very useful to assess the benefits of HHC when changing HHC parameters and/or rotor operational conditions.

The effect of HHC on rotor vibrations was estimated by means of a vibration quality criterion (GF), which was computed on-line from the 4/rev components of the forces and moments of the rotor balance, and which shows minima at the lowest vibration levels.

Rotor Operation

A scheme of the DLR digital higher harmonic control system is shown in Fig 4. Three computer-controlled, equally spaced electro-hydraulic actuators are used to move the swashplate in the desired way, in order to provide conventional pitch motion (collective and cyclic) as well as higher harmonic pitch motion (3P, 4P, 5P and any combination) for a precise blade root pitch control. For this four-bladed rotor, the higher harmonic pitch is achieved by superimposing 4P swashplate motion upon the basic swashplate collective and cylic (1P) flight control inputs. Collective 4P pitch motion (all four blades pitching simultaneously the same way) is provided as well as pitch schedules containing 3P, 4P and 5P pitch harmonic components, through proper phasing the 4P inputs (Refs 11,12,13). For this test computer-based manual HHC input, i.e. open loop control was used to generate the HHC signals. The system is also designed to operate at closed loop control.
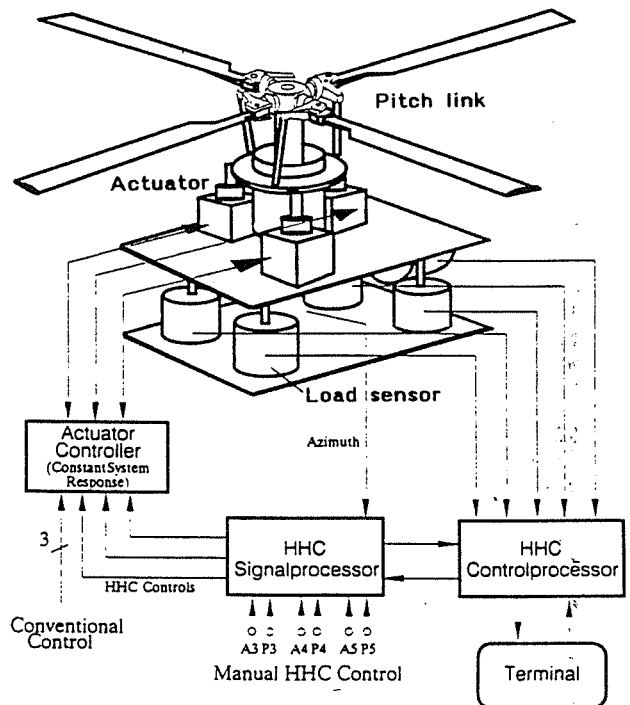

Fig 4 Scheme of HHC hardware.

The pitch motion achieved as well as the test procedure can be explained on the basis of Fig 5 which shows blade pitch angle data versus blade azimuth angle ψ for a specific simulated flight condition. For a given advance ratio μ and tip-path-plane angle α', the mean collective (6.0°, for the case shown) necessary to produce the required C_T and the basic 1P pitch (2.1°) for zero flapping trim with reference to the rotor shaft, were attained as shown. Once performance and acoustic data were acquired for this baseline case, pre- selected HHC pitch was superimposed to generate a deflection of θ_c at azimuth angle ψ_c and data were taken again. Due to the observed only minor variations in thrust coefficient and trim flight condition no adjustments were necessary in mean collective and cyclic pitch. The higher harmonic pitch portion (difference of total and baseline case pitch) is illustrated in Fig 5 (a) for a 4P HHC case.
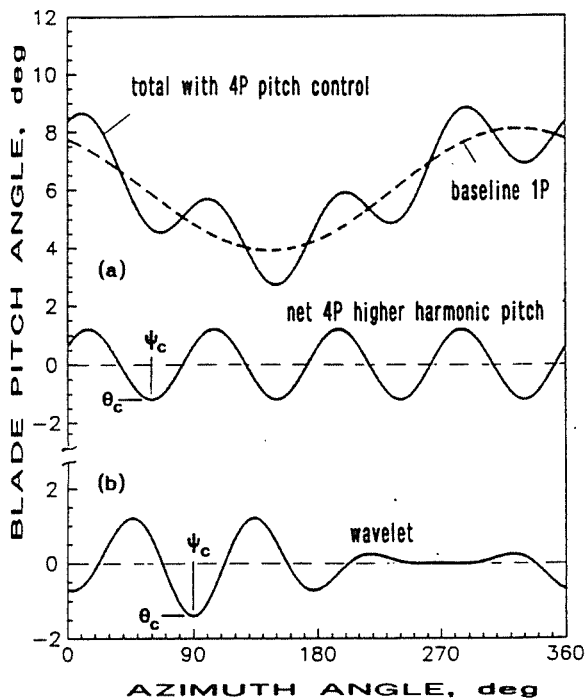

Fig 5   Superposition principle of higher harmonic blade pitch; (a) blade pitch angle θ versus azimuth for μ = 0.15, α' = 3.8°, C_T = 0.0044 at 4P HHC with θ_c = - 1.2° at ψ_c = 60°; (b) mixed mode HHC schedule (wavelet) with θ_c = -1.4° at ψ_c = 90°.

The net pitch in general is, due to normally occurring pitch-flap and pitch-lag couplings, not a purely 4P collective, but contains small portions of other harmonics as well. For the 4P noise data presented in this report, HHC amplitude θ_c and azimuth angle ψ_c in the first quadrant (0 $\leq$ ψ_c < 90°) are obtained from the 4P components (amplitude and phase) of the measured pitch angle FFT analyses. Similar considerations are valid for 3P and 5P pitch schedules with definition of the azimuth angle ranges of 0 $\leq$ ψ_c < 120° and 0 $\leq$ ψ_c < 72°, respectively. Also shown in Fig 5 (b) is the net higher harmonic pitch of a mixed mode case (combination of 3P, 4P, 5P modes) which was designed to form a wavelet with a pronounced negative HHC amplitude at one azimuth location and reduced higher harmonic pitch over a wide range of azimuth angles. This wavelet

approach was thought to be a first order approximation of individual blade control (IBC) and would allow an initial estimate of the effect of IBC on noise.

The tests were performed over a range of descent flight operating conditions where BVI is likely to occur with a few level flight conditions. These specific test "flight" conditions were defined by the tunnel referenced tip-path-plane angle α and the advance ratio μ. For the data presented, the tip-path-plane angles were corrected (Refs 22,23) to account for open jet wind tunnel effects to obtain equivalent freestream α' values. In order to relate the noise results to full-scale flight conditions of a BO-105 helicopter, equivalent descent angles θ were calculated based on a simplified force balance of Ref 23. For a few typical BVI test conditions the HHC parameters like mode, amplitude and phase were examined in detail; for a broader range of operating conditions only specific HHC parameters, expected to best reduce BVI noise, were examined.

TEST RESULTS

Change of Noise Characteristics by HHC

The effect of higher harmonic pitch control on BVI noise characteristics in the time and frequency domain is shown in Fig 6 for a "standard" operating condition (μ = 0.15, α' = 3.8°) equivalent to a low speed descent at θ = 6° glide slope with very intensive BVI noise generation. At part (a) of this figure contours of mid-frequency noise levels as measured for the baseline case without HHC (center) and for two higher harmonic pitch schedules are compared. Maximum advancing side BVI noise reduction (5-6 dB) is achieved at a nominal HHC schedule of 4-per-revolution, HHC amplitude θ_c =-1.2°, and phase angle ϕ = 30° (minimum HHC pitch at ψ_c = 53°) as shown in the right hand contour plot with annotation 4P/1.2°A/30°Ph, however at slightly increased retreating side BVI noise intensity. The noise directivity pattern appears also affected by HHC with the radiation lobe directed more towards the upstream direction for this case. Maximum retreating side BVI noise reduction (approx. 6 dB) is obtained for a similar pitch schedule (4P/1.2°A/ 180°Ph), however at a phase shift of 180° (ψ_c = 0°; left hand contour plot). In this case advancing side BVI noise is slightly reduced as well.

Related sound pressure time-histories (30 averages) for one rotor revolution and averaged frequency spectra for observer locations at maximum advancing side BVI (part (b)) and at max. retreating side BVI (part (c)) are arranged below the relevant contour plots for easy comparison. For the baseline case without HHC, the center column shows typical advancing side BVI sound pressure pulses of positive polarity and typical retreating side BVI noise pulses of negative polarity and lower amplitude. The related frequency spectra reveal a large number of blade passage frequency harmonics that indicate the dominance of BVI impulsive noise in the mid-frequency range. When HHC is initiated low-frequency loading noise is generated, which is apparent in the noise signatures and spectra, and the intensity of which is increased with HHC amplitude (θ_c).
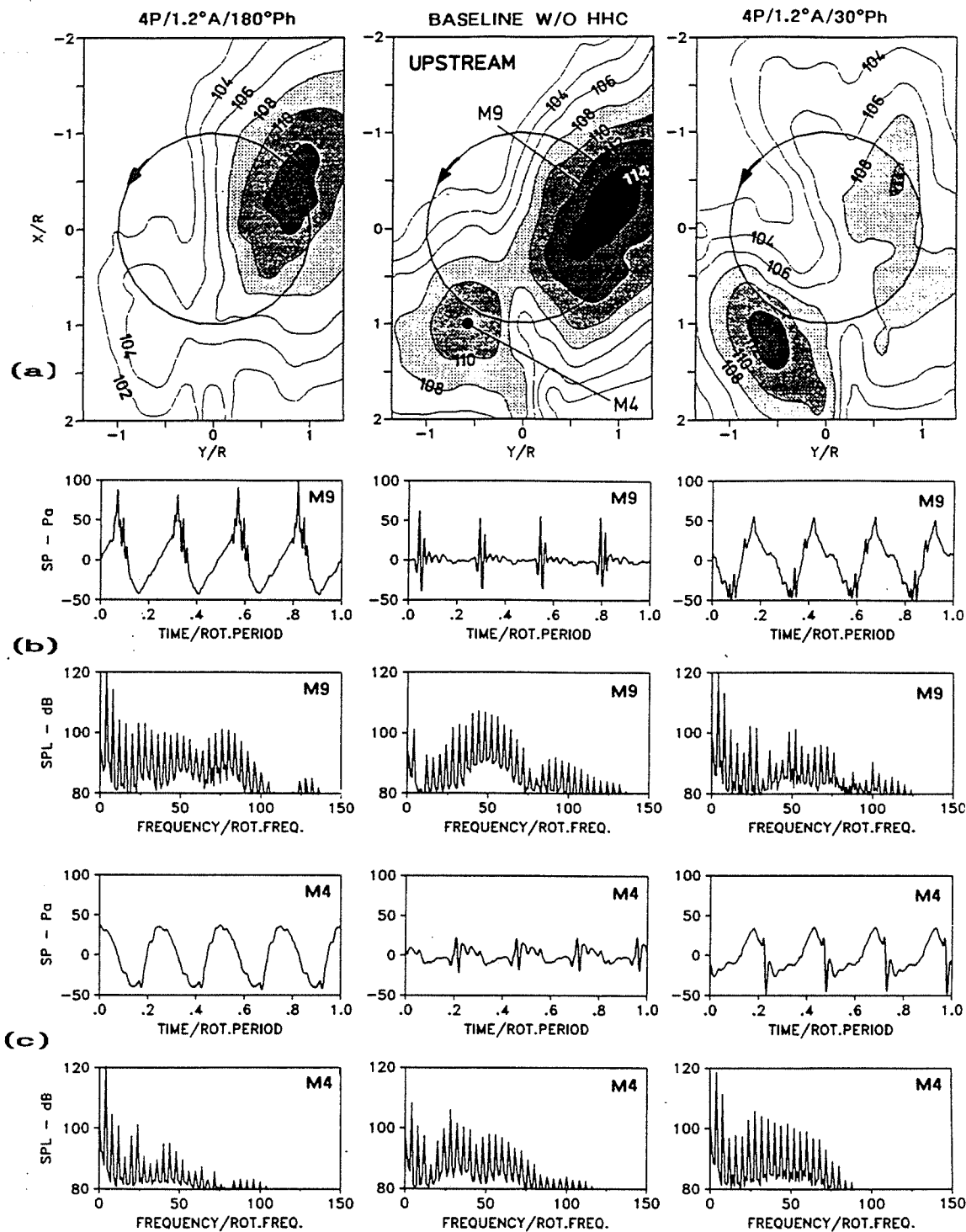
Fig 6 Effect of HHC on noise contours and BVI noise characteristics for low speed descent case of $\mu = 0.15$, $\alpha' = 3.8°$, $\Theta = 6°$, $C_T = 0.0044$, $M_H = 0.64$; (a) comparison of mid-frequency noise level contours; (b) comparison of advancing side BVI noise characteristics; (c) comparison of retreating side noise characteristics.

However, low frequency noise is not impor-
tant from a subjective weighted measure in
comparison to the mid-frequencies. Compari-
son of the BVI impulses, obvious in the
sound pressure time- histories, show largely
reduced BVI noise signatures for optimum
control settings for advancing side BVI and
retreating side BVI, respectively. The re-
levant comparison of the frequency spectra
reflect the decrease in mid-frequency noise
levels for optimum HHC control settings at

increased low frequency noise. In general,
the measured sound pressure time histories
at a fixed observer location, where strong
advancing side BVI is radiated, indicate
that variation of HHC phase results in dra-
matic changes of the BVI waveform shapes.
This is shown in Fig 7 for one rotor revo-
lution and constant rotor operating condi-
tions for the "standard" BVI case. For the
baseline case without HHC, one strong BVI
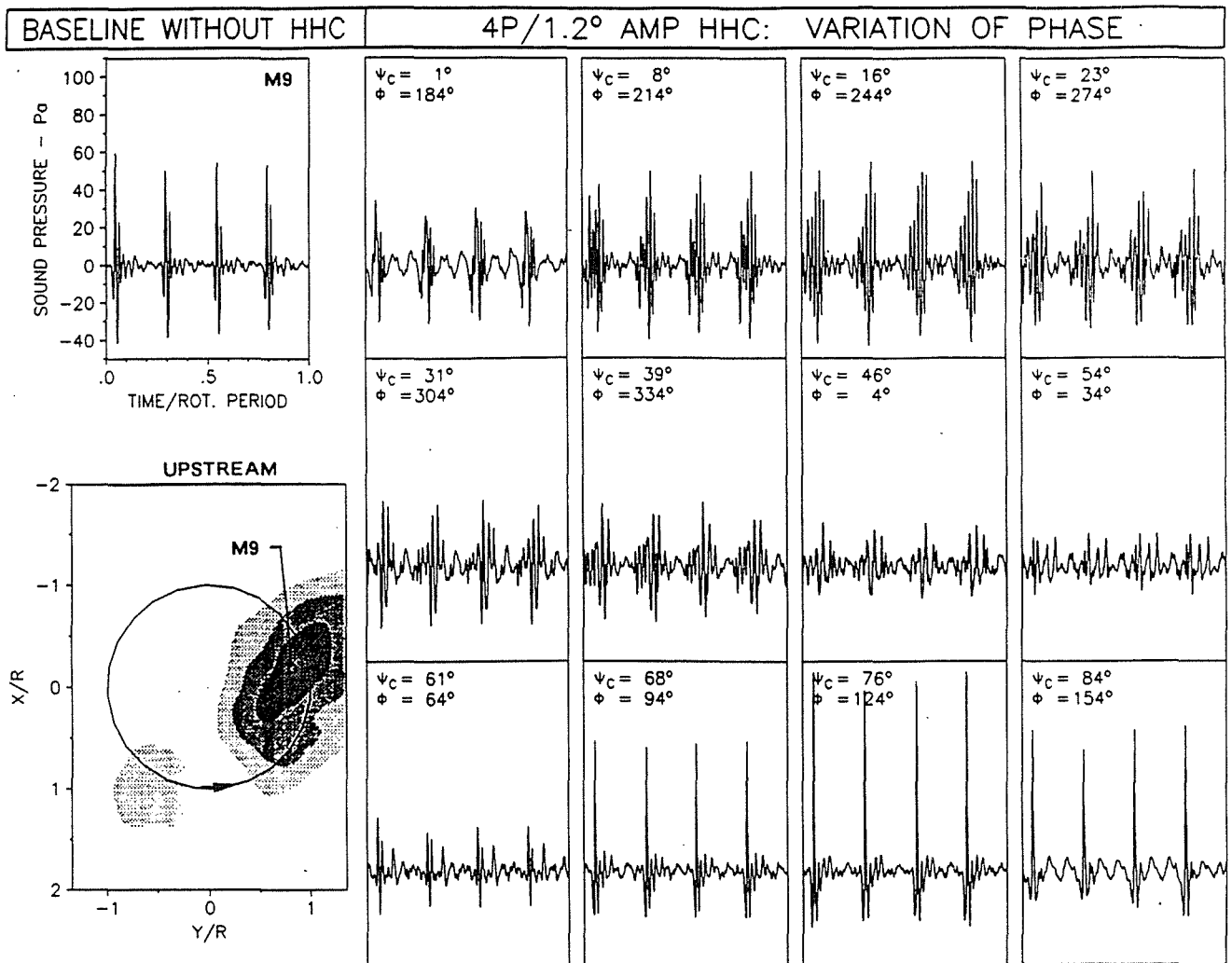impulse is seen. With HHC (4P/1.2°A) acti-

Fig 7 Change of BVI impulsive noise wave-forms with HHC phase angle variation at 4P/1.2° amplitude pitch control; acoustic data (except baseline) are high-pass filtered at 200 Hz; rotor condition as for Fig 6 (6°-descent).

vated, multiple BVI waveforms (up to 5 impulses) appear at certain HHC phase angles as well as waveform shapes with one very strong impulse at other phases. Very weak impulses are found at a specific azimuth phase angle ψ_c = 54° that corresponds to the optimum noise reduction control phase angle for this HHC pitch mode. Similar trends are observed for other HHC schedules.

The change of HHC phase is obviously changing the interaction geometry (blade position and vortex trajectories) due to the modified blade loading and blade motion. Thus, it appears that in some cases, the blade encounters up to five of the seven vortices, which are present in the first quadrant at this descent condition (Ref 8). At another control phase, it very intensely hits only one vortex, and finally and most desired, the blade seems to miss them all with the effect of largely reduced BVI noise. CAMRAD-JA calculations using a free-wake formulation indicate distinct changes of the interaction geometry when, for a specified HHC pitch schedule, the control phase is changed. The locations, where the vortex system is predicted to cut through the rotor disk (possible BVI source locations) appear to be correlated in a non-linear way with the con-

trol phase. This is shown in Fig 8, where the vertical wake-blade displacements (at Y/R = 0.87) are plotted vs streamwise position X/R for the standard baseline case and
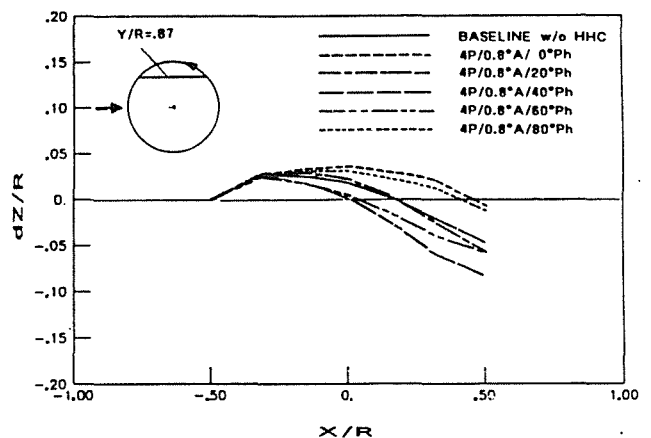

Fig 8 Predicted vertical blade-wake displacements for baseline (w/o HHC) and for 4P/0.8°A HHC pitch schedule at different phase angles as seen in a vertical plane parallel to the flow direction intersecting the rotor disk at Y/R = 0.866. Rotor condition for Fig 6.

4P/0.8°A pitch control at various phase angles. Possible BVI source locations (dZ/R = 0) show substantial changes in upstream and downstream directions. Consequently, the intensity and direction of sound radiation from the acoustic source locations is subjected to similar, apparently non-linear changes, as is seen in the BVI waveforms of Fig 7 for a fixed microphone location.
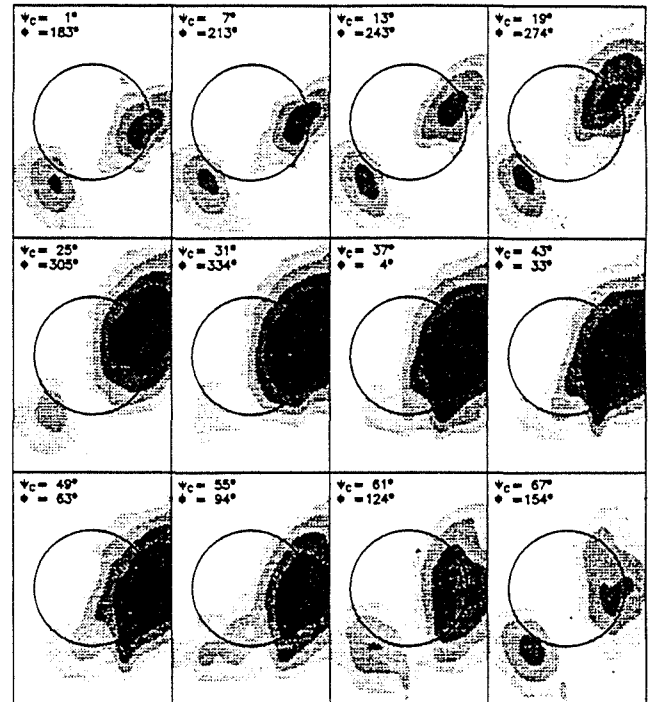
Effect on BVI Noise Directivity

The resulting changes in the noise radiation directivity pattern of the complete sound field underneath the rotor plane is shown in Figs 9 (a) - (d) for the typical BVI "standard" operating case of low speed descent

(μ = 0.15, Θ = 6°). To emphasize the more important radiation lobes only the higher noise levels have been plotted. Series of mid-frequency noise level contour plots for different higher harmonic pitch control phase angles are compared to the directivity pattern of the baseline case (part (d)). HHC pitch schedules of 3P/0.8°A (part (a)), of 4P/0.8°A (part (b)), and of 5P/0.8°A (part (c)) are presented with variation of the control phase (ϕ) at increments of 30 degrees. The contour plots are arranged in such a way, that the plot with the lowest azimuth angle of minimum HHC pitch (Ψ_c) appears first. Azimuth and control phase angles (based on measured values) are noted on each plot.
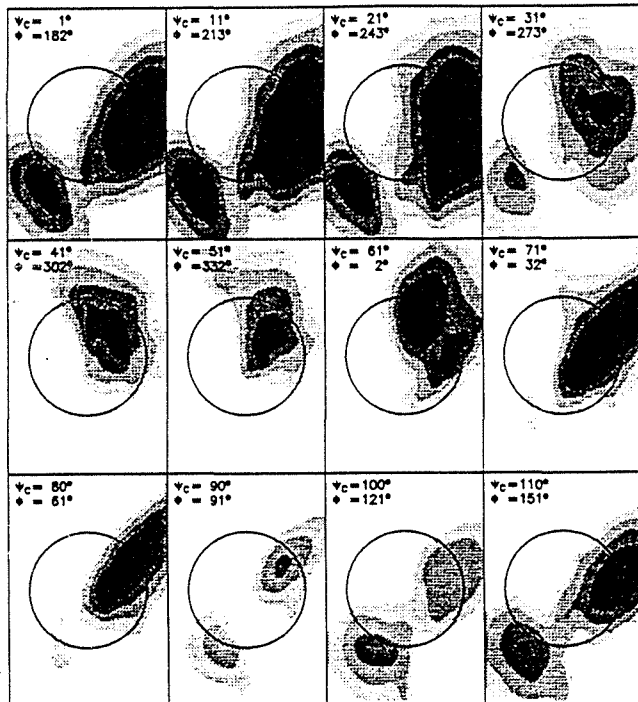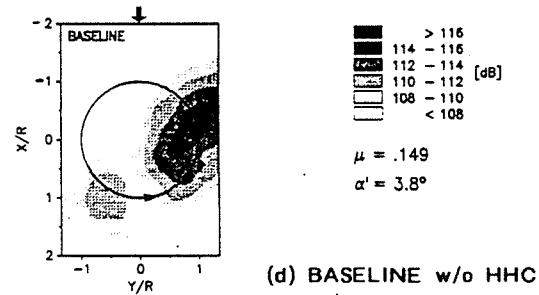

(a) 3P/0.8°AMP

(c) 5P/0.8°AMP

(b) 4P/0.8°AMP

■	> 116
■	114 – 116
▨	112 – 114 [dB]
▨	110 – 112
▨	108 – 110
□	< 108

μ = .149

α' = 3.8°
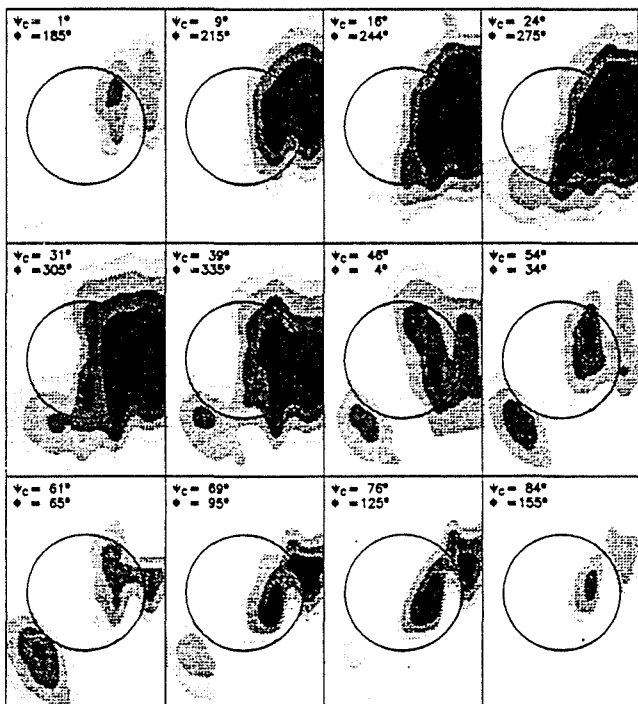
(d) BASELINE w/o HHC

Fig 9   Change in BVI noise directivity with HHC variations for the low speed descent condition of Fig 6; (a) variation of HHC phase at 3P/0.8° amplitude; (b) variation of HHC phase at 4P/0.8° amplitude; (c) variation of HHC phase at 5P/0.8° amp.; (d) baseline.

As compared to the baseline case, strong changes in BVI noise radiation intensity and direction are observed for all HHC pitch schedules (3P, 4P, 5P), when the pitch control phase is varied. In particular, for the 3P pitch schedule (Fig 9 (a)) the minimum HHC pitch azimuth angle Ψ_c is shifted through the first quadrant and partly
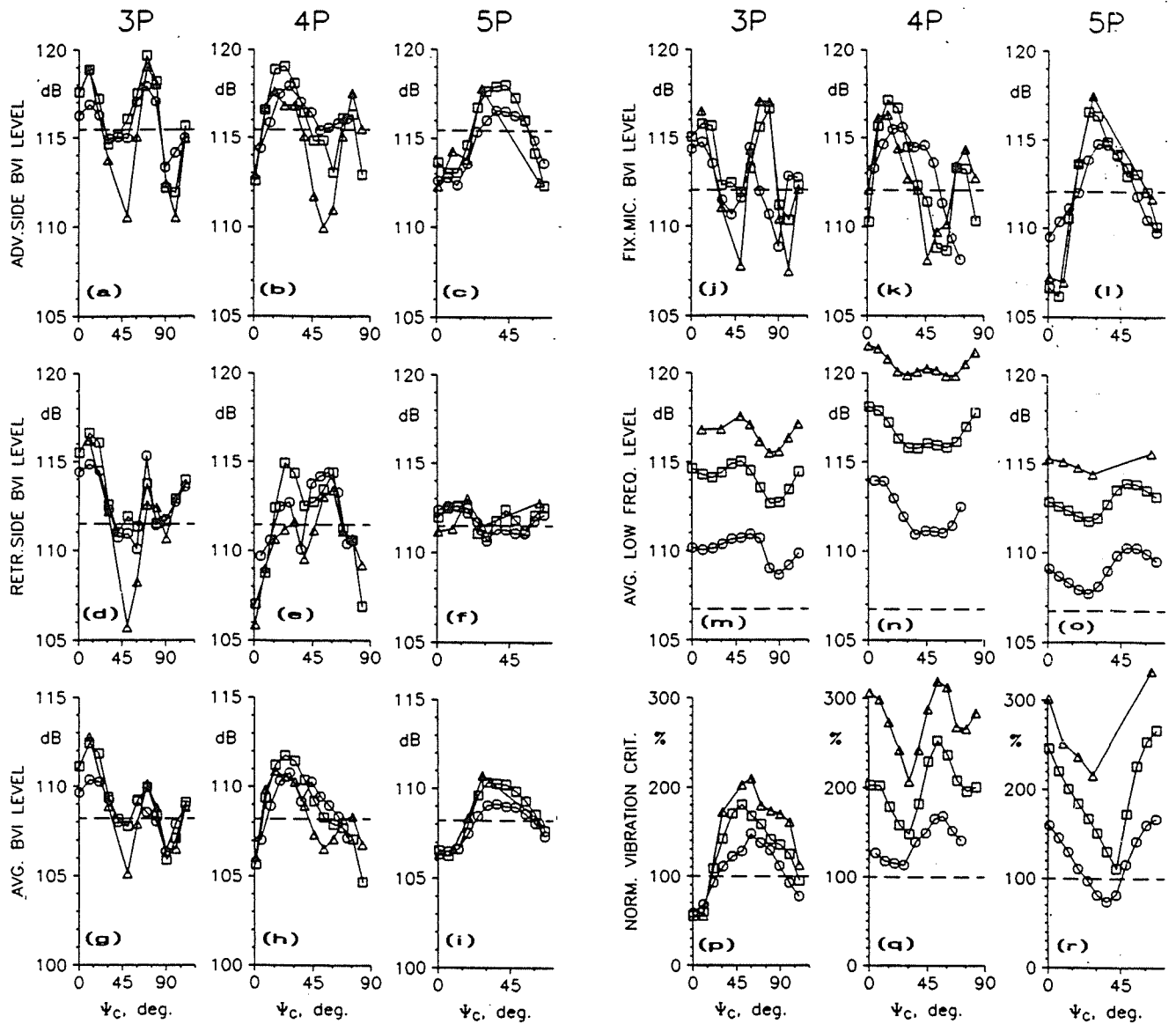
Fig 10 Variation of noise and vibrations with HHC parametric variations for the low speed descent condition of Fig 6; baseline w/o HHC:----; symbols are for θ_c = -0.4° (nominal), O ; for θ_c = -0.8°, □ ; and for θ_c = -1.2°, △ . (a) - (f) mid-frequency (6 to 40 f_{bp}) max. noise level vs ψ_c at 3P, 4P, 5P control mode; (g) - (i) mid-frequency average noise level; (j) - (l) mid frequency noise level at fixed microphone position (M9 of Fig 6); (m) - (o) low-frequency average noise level; (p) - (r) normalized vibration criterion.

through the second (0° ≤ ψ_c ≤ 120°), when the phase angle is modified from 0° to 360°. Largely increased advancing and retreating side BVI noise radiation is seen at lower ψ_c-values (0° ≤ ψ_c ≤ 30°) with a direction-al change towards the flight direction. At higher ψ_c-values (30° < ψ_c < 70°), retreating side BVI is effectively reduced at slightly decreased levels of advancing side BVI, which appears more focussed towards the flight track and even extending into the retreating side. At ψ_c values above 70° the directivity patterns become similar to the baseline case with increased advancing side BVI at 70° and 80° azimuth. Effectively reduced advancing side BVI is obtained for ψ_c-values about 90° and 100°, at retreating side BVI levels comparable with the baseline case. For the 4P HHC mode (Fig 9 (b)) the azimuth angle of minimum HHC pitch is shifted through the first quadrant (0 ≤ ψ_c ≤ 90°). Again dramatic changes of the BVI noise directivity is observed. Most effective reductions of advancing and retreating

side BVI noise (at the order of 4 dB) is obtained for ψ_c-values about 80° and 90° (or 0°). At 5P control mode (Fig 9 (c)) the minimum HHC amplitude is shifted through the azimuthal range 0° ≤ ψ_c ≤ 72° for one complete HHC period. The directivity of BVI noise radiation is similar to the baseline case, however the noise intensity again shows strong variations. Moderate reductions of advancing side BVI noise is measured for minimum HHC pitch azimuth angles of 60 ≤ ψ_c ≤ 90°, at nearly unchanged retreating side BVI noise levels (bearing in mind that the azimuthal range 72 ≤ ψ_c ≤ 90° is equivalent with 0 ≤ ψ_c ≤ 18°).

At other rotor operating conditions known to generate BVI noise, similar changes of the mid-frequency noise directivity patterns are observed when the HHC pitch schedule, in particular the HHC phase, is varied. At higher HHC amplitudes the directivity changes are even more pronounced.

Effect on Noise Levels and Vibration

The mid-frequency noise level contours and noise characteristics as well as the noise directivity patterns shown, have indicated strong variations due to changes of the HHC parameters. To more clearly demonstrate how operational pitch control variations affect rotor noise and vibrations, the general trends and the noise reduction potential of HHC are illustrated in Figs 10 (a) - (r), which summarize the results of the HHC parametric variations and allow a quantitative evaluation of its effects. Selected noise evaluation measures (mid-frequency, low-frequency) and a vibration criterion are plotted for different HHC modes (3P, 4P, 5P) and HHC amplitudes (θ_c = -0.4°, -0.8°, -1.2°) versus rotor azimuth angle of minimum HHC amplitude (ψ_c). The data for the base-line case without HHC corresponding to the standard (6° descent) rotor operating condition, is indicated on each plot by a dashed line. Advancing and retreating side maximum, mid-frequency noise levels have been determined separately, from the measurement plane underneath the first to the third quadrant and underneath the fourth quadrant, respectively.

Figs 10 (a)-(c) present maximum advancing side BVI noise levels at 3P, 4P and 5P HHC, respectively. Effective noise reductions but also increased noise levels are seen for all three control modes. For 3P and 4P HHC the larger control pitch amplitude of θ_c = -1.2° produces the larger noise reductions. For 3P HHC noise reductions (order of 6 dB) are obtained for minimum HHC pitch in the range of 40° $\leq \psi_c \leq$ 50° and 90° $\leq \psi_c \leq$ 100°. At 4P HHC optimum noise control is achieved for 50° $\leq \psi_c \leq$ 60° and again for ψ_c = 90° (or 0°). At 5P HHC smaller noise reductions (almost independent of HHC amplitude) are observed at a wider azimuth angle range of 72° $\leq \psi_c \leq$ 90° (or 0° to 18°). Very impressive noise reductions and similar trends are seen for retreating side BVI as shown in Figs 10 (d)-(f). Maximum reductions (approx. 6 dB) are measured for the largest HHC amplitude (1.2°) for 3P at ψ_c = 50° and for 4P at ψ_c = 90° (or 0°). Moderate reductions are found at about ψ_c = 80° (3P) and about ψ_c = 40° (4P). 5P control appears to be less effective. On close inspection of the 3P and 4P control results (Figs 10 (a), (d) and (b), (e)), it is obvious that the azimuth angles ψ_c (or equivalent the control phase angles) for effective noise reductions are slightly different for advancing side and retreating side BVI. This implies that both noise sources cannot be simultaneously controlled in an optimal way by HHC for the considered test case.

The spatial average mid-frequency noise levels (part (g)-(i)) representing the BVI noise of the complete measurement plane, therefore indicate somewhat less reductions (order of 3 - 4 dB). Also, it appears that average mid-frequency noise can be effectively reduced at moderate HHC amplitudes (e.g. θ_c =-0.8) with the minimum HHC amplitude at about ψ_c = 90° for each control mode. The mid-frequency BVI noise levels for a fixed upstream microphone location (mic 9 at X_w/R= -0.75), chosen to receive maximum advancing side BVI noise radiation at the baseline case (part (j)-(l)) show similar trends as for the maximum advancing side BVI

(see part (a) -(b)) except for 5P control mode, where larger reductions are obtained, possibly an effect of directivity changes due to HHC.

The BVI noise measured by the fuselage and by the inflow-traverse microphones is due to the observed directivity changes subjected to substantial changes of the degree of correlation.

Spatial averaged low frequency noise levels are presented in Figs 10 (m)-(o). Compared with the baseline case, they are largely increased with application of HHC, distinctly growing with HHC amplitude. The highest levels are observed at 4P control (plus 13 to 15 dB at 1.2° amplitude), the lowest at 5P (7 to 8 dB). It is important to note, that on the subjective A-weighted dB scale, the low frequency noise is not of concern compared to the mid-frequency BVI noise. For example, the blade passage frequency of 70 Hz must be attenuated by at least 25 dB on the dBA scale, when compared with the mid-frequency (BVI) harmonics.

The vibration quality criteria calculated from the 4P components of the six-component balance forces and moments and normalized to the baseline case vibrations, are shown in Figs 10 (p)-(r). Inertial forces due to the accelerating masses of the swashplate, blade root hardware, actuator pistons, and other control hardware used to produce the HHC pitch motion have been compensated for (inertial effects removed) by proper calibration. In general increased vibration levels are seen at reduced BVI noise control settings and lower levels when mid-frequency noise is increased. This is quite consistent with the findings in Refs (14, 16, 17). The larger the HHC amplitude the higher are the vibration levels. However, for 3P pitch control a number of control settings are found for simultaneous noise and vibration reduction (see parts (a,g and p)). Also, the absolute vibration levels do not appear prohibitive in this low speed descent flight regime, where the application of HHC for noise reduction would be most effective. Furthermore, the mixed mode HHC may offer a possible solution of reducing BVI noise without increasing vibrations. As shown in Fig 11, for a combined 3P, 4P and 5P HHC schedule at -1.4° amplitude (see wavelet of Fig 5) with minimum HHC pitch at ψ_c = 0° a mid-frequency noise reduction of 4.5 dB is achieved at only 50% increased vibration level. A separate paper reporting on further investigations into the HHC effect on vibratory loads in the fixed and rotating frame at optimum noise reduction control is planned.

Variation of Flight Condition

Descent angle variation:

The isolated effect of descent angle change, or equivalently, variation of the tip-path plane angle on the mid-frequency, maximum advancing side BVI noise level and the effectiveness of HHC to reduce those levels are presented in Fig 12. α was changed in increments of 0.5° and all other test conditions were held constant. Baseline case levels are compared with results of a specific and effective HHC pitch schedule of 4P/0.8°A/180°Ph (ψ_c = 0). The baseline cases
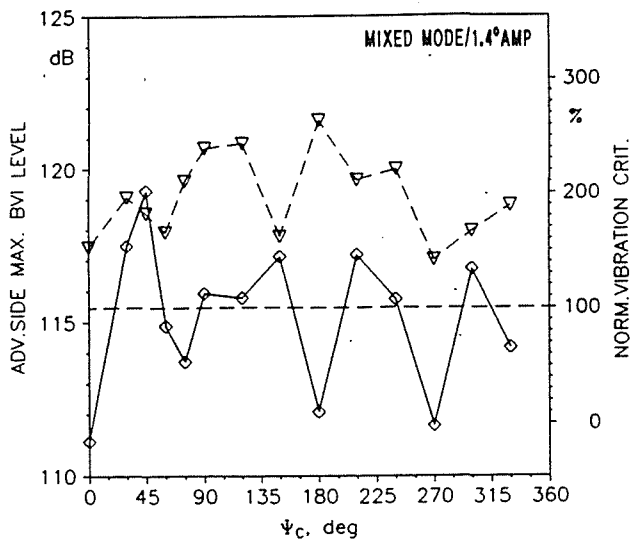
Fig 11 Variation of advancing side mid-frequency maximum noise level and normalized vibration criterion with azimuth ψ_c for the mixed mode HHC wavelet (3P, 4P, 5P and $\theta_c = -1.4°$) of Fig 5 (b). Rotor condition: 6° descent, $\mu = 0.15$.

indicate maximum BVI noise generation between 6° and 7° descent angle at constant advance ratio ($\mu = 0.15$). The application of HHC at these fixed control settings yield maximum noise reduction (approx. 5 dB) at about $\theta = 7°$, and then starts to be less effective at other descent angles (or descent rates). At low descent angle and less intense BVI noise the application of this specific HHC schedule has a negative effect on noise (increase). Blade dynamic response to HHC may be forcing the rotor wake closer to the rotor disc thus increasing BVI noise,
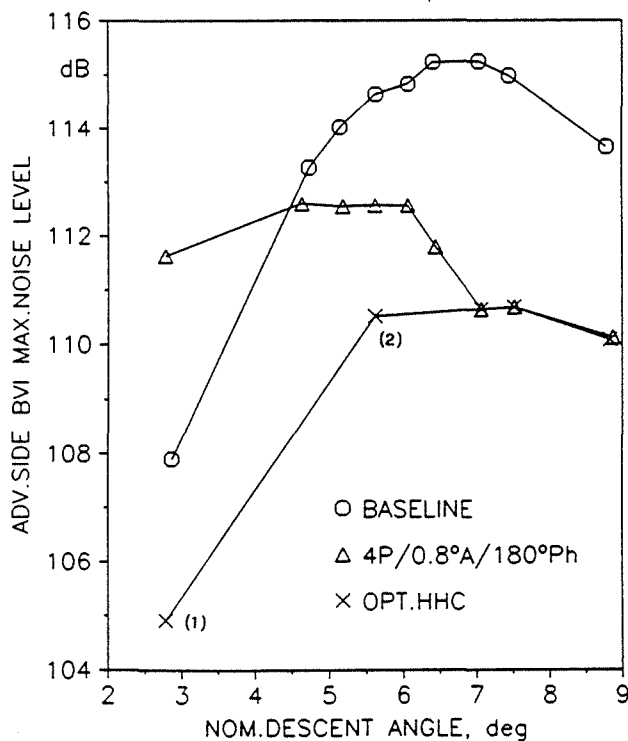

Fig 12 Effectiveness of a fixed HHC pitch schedule (4P/0.8°A/180°Ph) to reduce adv. side BVI max. noise levels over a range of descent angles at constant advance ratio ($\mu = 0.15$).

when HHC is applied. By modifying the HHC schedule (changing to 3P control, enlarging HHC amplitude and/or changing phase) BVI noise is further reduced as illustrated in Fig 12. In order to guarantee optimum noise reduction at different descent flight conditions, the development of a closed-loop algorithm is considered necessary.

Variation of advance ratio:

Variation of rotor operating conditions, limited to low speed and moderate speed descent, has shown that a noise reduction benefit is obtained for a range of descent flight conditions known to generate strong BVI. The noise reductions measured for a fixed 4P HHC pitch schedule with $\theta_c = -0.8°$ at $\psi_c = 0°$ ($\phi = 180°$) are illustrated in Fig 15, where the mid-frequency maximum
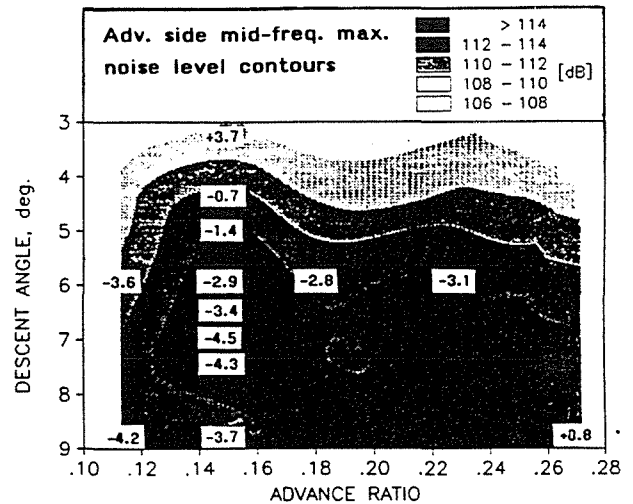

Fig 13 Mid-frequency maximum noise level contours versus flight condition for the baseline (no HHC) case. Negative numbers indicate noise reductions due to HHC (4P/0.8°A/180°Ph).

noise level contours for the baseline (no HHC) case are plotted versus flight condition. The overlaid numbers (negative for reduction) indicate the noise reduction benefit, which is highest at low speed descent. This is consistent with Ref 16. At high speed descent or at low speed, less steep descent increased noise levels are observed, however when the pitch schedule is changed (e.g. to higher θ_c), a noise benefit is obtained for these flight conditions as well.

CONCLUSIONS

(1) This model rotor wind tunnel study clearly demonstrates the benefit of HHC to reduce BVI impulsive noise over the range of descent conditions where BVI noise is most intense. Highest mid-frequency noise reductions (locally more than 6 dB) are measured at low speed descent condition (similar to the noise certification landing approach). More limited or no noise benefit is seen for flight conditions outsite the intensive BVI range.

(2) The detailed acoustic in-flow measurements in the anechoic environment of the DNW

open test section reveal large changes of the BVI impulsive noise characteristics and noise directivity patterns with HHC varia-tions (especially phase variations).

(3) Mid-frequency level contour plots show reductions of advancing side and retreating side BVI maximum noise levels of similar magnitude (about 6 dB) for specific HHC pitch schedules, however, at different HHC phase angles. The noise reductions corres-pond to reductions in blade pitch at speci-fic azimuth angle regions between 40° and 90° (adv. side BVI) and between 270° and 300° (retr. side BVI). 3P and 4P HHC modes are more effective than 5P. The largest re-ductions are obtained at the largest HHC am-plitude (θ_c = -1.2°). Spatial averaged mid-frequency noise reduction (3-4 dB) is somewhat less due to noise directivity changes.

(4) The use of HHC produces increased low frequency loading noise, which however ap-pears to be of minor concern when a subjec-tive A-(or NOY)-weighted measure is consi-dered. Also, vibrational loads increase, es-pecially at HHC schedules most benefitial for BVI noise reduction. But the levels do not appear prohibitive in the low speed flight regime, where the use of HHC for noise reduction would be most effective. Fi-nally, a number of control settings are found for simultaneous noise and vibration reduction.

(5) The mixed mode HHC wavelet approach tested does not significantly improve BVI noise reduction, however, may have a poten-tial to combine both, BVI noise reduction and low vibration levels.

(6) Rotor simulation results (at 5° azimuth-al resolution, Ref 14) give some evidence that BVI noise reduction is due to decreased blade loading in the azimuthal regions of the first and fourth quadrant (specified in (3)) where strong BVI is known to occur. Nothing definite can be said about the in-fluence of vortex strength, since it is pre-dicted to be partly increased and partly de-creased. Blade-vortex displacements are de-finitely affected by HHC and evidently re-present a dominant factor in the BVI noise reductions. A high resolution air load code ($\leq$ 1° azimuth) may provide a better insight into the occurrences.

(7) Individual blade control (IBC) is seen to be a highly desirable control capability, that could be used to tailor the blade pitch schedule to local azimuth ranges, such as regions where tip vortices are shed and where blade-vortex interactions occur, and thus to try to combine low vibration loads with optimum noise reductions on the advanc-ing and retreating side simultaneously.

(8) For effective noise reduction at vari-able descent flight conditions different HHC schedules are necessary, that suggest the use of an adaptive closed-loop control algo-rithm with the need for representative feed back signals from fuselage and/or blade mounted sensors.

(9) Non-intrusive local wake and blade posi-tion measurements (e.g. use of LDV) are strongly recommended in order to determine both, the blade-vortex displacements gene-rated by HHC and the tip vortex strenghts during BVI. Finally, blade surface pressure measurements would make-up the set of infor-mation necessary to improve the understand-ing and modelling of the effect of HHC on BVI noise generation and reduction.

REFERENCES

1 Schmitz, F.H.; Boxwell, D.A.: In-flight far-field measurement of helicopter impul-sive noise. J. Amer. Hec. Soc., Vol. 21, No. 4, 1976.

2 Boxwell, D.A., Schmitz, F.H.: Full- scale measurements of blade/vortex interaction noise. J. Amer. Helic. Soc., Vol. 27, No. 4, 1982.

3 Cox, C.R.: Helicopter rotor aerodynamic and aeroacoustic environments. AIAA 77-1338, 1977.

4 Schlinker, R.H.; Amiet, R.K.: Rotor-vor-tex interaction noise. NASA CR 3744, 1983.

5 Splettstoesser, W.R.; Schultz, K.-J.; Boxwell, D.A.; Schmitz, F.H.: Helicopter model rotor blade/vortex interaction impul-sive noise: scalability and parametric va-riations. NASA TM 86007, 1984.

6 Martin, R.M.; Splettstoesser, W.R.; Elliott, J.W.; Schultz, K.-J.: Advancing side directivity and retreating side inter-actions of model rotor blade- vortex inter-action noise. NASA TP 2784, AVSCOM TR 87-B3, 1988.

7 Hoad, D.R.: Helicopter blade-vortex in-teraction locations: scale-model acoustics and free-wake analysis results. NASA TP 2658, 1987.

8 Splettstoesser, W.R.; Schultz, K.-J.; Martin, R.M.: Rotor blade-vortex interaction impulsive noise source identification and correlation with wake predictions. AIAA-87- 2744, 1987.

9 Hardin, J.C.; Lamkin, S.L.: Concepts for reduction of blade-vortex interaction noise. AIAA-86-1855, 1986.

10 Wood, E.R.; Powers, R.W.; Hammond, C.E.: On methods for aplication of harmonic con-trol, Vertica, Vol.4, pp.43-60, 1980.

11 Lehmann, G.: The effect of HHC to a four bladed hingeless model rotor. Paper 64, Proc. Tenth European Rotorcraft Forum. The Hague, The Netherlands, 1984.

12 Lehmann, G.: Untersuchungen zur höherharmonischen Rotorblattsteuerung bei Hubschraubern. DFVLR-FB 87-36, 1987.

13 Lehmann, G.; Kube, R.: Automatic vibration reduction at a four bladed hingeless model rotor - a wind tunnel demonstration. Paper 60, Proc. Fourteenth European Rotorcraft Forum, Milano, Italy, 1988.

14 Splettstoesser, W.R.; Lehmann, G.; van der Wall, B.: Higher harmonic control of a helicopter rotor to reduce blade- vortex interaction noise. Z.F.W. (Zeitschrift für Flugwissenschaften), Vol. 14, pp. 109 - 116, 1990. (See also Proceedings of the 15th European Rotorcraft Forum, Sept. 1989).

15 Brooks, T.F.; Booth, E.R.; Jolly, J.R.; Yeager, W.T.; Wilbur, M.L.: Reduction of blade-vortex interaction noise through higher harmonic pitch control. J.A.H.S., Vol. 35, No. 1, pp. 86-91, Jan. 1990. (See also NASA TM-101624/ AVSCOM TM 89-B-005, July 1989).

16 Brooks, T.F.; Booth, E.R.: Rotor blade-vortex interaction noise reduction and vibration using higher harmonic control, Paper No. 9.3, Proc. 16th Europ. Rotorcraft Forum, Glasgow, U.K., 1990.

17 Polychroniadis, M.: Generalized higher harmonic control, ten years of Aerospatiale experience, Paper III 7.2, Proc. 16th Europ. Rotorcraft Forum, Glasgow, U.K., 1990.

18 Van Ditshuizen, J.C.A.; Courage, G.D.; Ross, R.; Schultz, K.-J.: Acoustic capabilities of the German-Dutch Wind Tunnel, DNW. AIAA-83-0146, Jan. 1983.

19 Langer, H.-J. (SCITRAN, transl.): DFVLR rotorcraft-construction and engineering. NASA TM-77740, 1984.

20 Breustedt, W. (SCITRAN, transl.): Data analysis on the rotor test stand program for interactive processing. NASA TM-77948, 1985.

21 Martin, R.M.; Splettstoesser, W.R.; Elliott, J.W.; Schultz, K.-J.: Advancing-side directivity and retreating-side interactions of model rotor blade-vortex interaction noise. NASA TP-2784, AVSCOM TR 87-B-3, 1988.

22 Heyson, H.H.: Use of superposition in digital computers to obtain wind-tunnel interference factors for arbitary configurations, with particular reference to V/STOL models. NASA TR R-302, 1969.

23 Brooks, T.F.; Jolly, J.R.; Marcolini, M.A.: Helicopter main rotor noise-determination of source contributions using scaled model data. NASA TP-2825, August 1988.